NANO LETTERS

2008
Vol. 8, No. 6
1590-1595

Nonlinear and Nonplanar Dynamics of Suspended Nanotube and Nanowire Resonators

William G. Conley,[†] Arvind Raman,[*,‡] Charles M. Krousgrill,[§] and Saeed Mohammadi[||]

School of Mechanical Engineering and Birck Nanotechnology Center, School of Mechanical Engineering and Birck Nanotechnology Center, School of Mechanical Engineering, School of Electrical Engineering and Birck Nanotechnology Center, Purdue University, West Lafayette, Indiana 47907

Received December 29, 2007; Revised Manuscript Received March 7, 2008

ABSTRACT

Previous works on suspended carbon nanotube and nanowire resonators assume a priori that they oscillate in a single plane. We explore the nonlinear dynamics of such resonators and demonstrate that they can suddenly transition from a planar motion to a whirling, "jump rope" like motion. We identify nondimensional gate voltage, resonator geometry, quality factor, and flexural and axial elastic stiffnesses for which such motions can arise. The deliberate use of nonlinear and nonplanar motions opens up a variety of new modalities for this class of nanoelectromechanical systems that are not accessible in the linear operating regime.

Nanotube or nanowire resonators consist of a carbon nanotube (CNT) or a slender nanowire suspended over a trench and excited via electrostatic or magnetomotive forces. The high-frequency mechanical oscillation is detected either as a variation of the source−drain current[1] or through electromagnetic induction.[2] These devices are said to be "self-sensing" because the actuation and measurement occur simultaneously and directly.

Such resonators have gained increased interest for their potential applications as sensors and as circuit elements. Due to their small mass and high stiffness, the mechanical resonance frequencies of such devices are very high[1,3−6] ensuring high bandwidth, ultrafast response, and low power consumption. Additionally, the gate electrode can actively modify the pretension allowing for a tunable, high-quality factor nanoresonator that could replace radio frequency (RF) circuit elements such as filters, mixers, demodulators, electronic oscillators, and frequency synthesizers. Recently a single nanotube resonator replaced four circuit building blocks of a radio receiver.[7] Eventually, a combination of nanoresonators, nanotube based nonvolatile memories,[8] and nanotube/nanowire transistors can be used to implement all analog, digital, and RF electronic functions without a need for bulky inductors and capacitors. The tiny mass of nanotube and nanowire resonators also implies that they can serve as mass detectors[4] for chemical and biological sensing applications with ultimate mass detection limits that greatly exceed the capabilities of microcantilever mass sensors.[9]

In an effort to guide the rational development of nanotube and nanowire resonators, several groups have modeled the linear vibrations of such devices. Linear, classical thin beam theory has been used to predict the resonance frequencies of single and multiwalled carbon nanotube resonators[3,10] and of nanotube bundles.[11] In order to bring theoretical predictions closer to experimental measurements, these models have been modified to account for initial slack[12] as well as initial tension.[5,13]

As the excitation magnitude is increased, nanotube and nanowire resonators display distinct nonlinear characteristics. Early experiments[1,2] indicated the presence of hysteretic jumps in source−drain current modulation as the drive frequency was swept up and down across resonance. The existence of nonlinear jump phenomena implies that the effective resonance bandwidth of such devices can be altered due to the presence of nonlinearities.[14] Theoretical models of this nonlinear behavior have focused on determining the backbone curve of the response[15] or the frequencies at which

* Corresponding author, raman@ecn.purdue.edu.
† School of Mechanical Engineering and Birck Nanotechnology Center.
‡ School of Mechanical Engineering and Birck Nanotechnology Center.
§ School of Mechanical Engineering.
|| School of Electrical Engineering and Birck Nanotechnology Center.

10.1021/nl073406j CCC: $40.75
Published on Web 05/20/2008

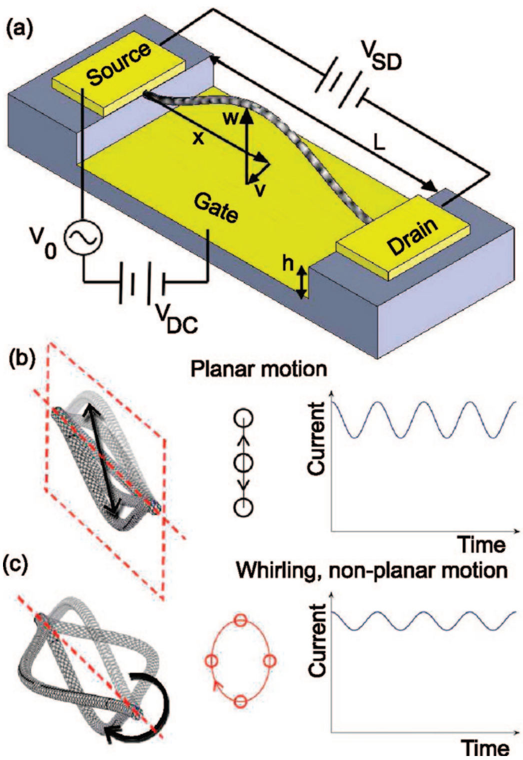

Figure 1. (a) Schematic of a nano-oscillator of diameter d and length L suspended above a trench of depth h. For measurement purposes, a source−drain voltage of V_{SD} is applied across the nanotube. The deflections at a point x along the length are v (horizontal) and w (vertical). A forcing voltage $V_g = V_{dc} + V_0\cos(\Omega\tau)$ is applied at the gate electrode. (b) A schematic depicting the planar response of the oscillator resulting in a large modulation of the source−drain current. (c) A schematic depicting the nonplanar response of the oscillator which can arise at larger driving voltages and at certain driving frequencies.

jumps occur.[16] More recently the domains of attraction of different oscillatory steady-state solutions of a nanowire resonator have been studied theoretically and experimentally.[15]

Up to now, all the published works on nanotube and nanowire resonators assume a priori that the nanotube or nanowire oscillates within a fixed plane. However, a nanowire or a nanotube possesses two spatially orthogonal vibration modes with nearly identical frequencies. It is natural to ask the question whether a nanotube or nanowire excited in one plane can interact nonlinearly with its orthogonal mode to create whirling or jump-rope like motions. Such nonplanar motions are known to occur in guitar-like macroscopic strings that are forced in a single plane.[17−19] The onset of such nonplanar motions is of great interest for the reliability of suspended nanotube or nanowire resonators and may also offer new opportunities for sensing, memory, and filter modalities.

In this work we develop a nonlinear elastic beam model for an electrostatically or magnetomotively excited nanotube or nanowire and derive closed form analytical criteria for (a) the onset of nonlinear jump phenomena for planar motion and (b) the onset of nonplanar, whirling motions. Because these criteria contain material and geometric properties of the resonators, we are able to generate parameter space diagrams using nondimensional parameters that clearly differentiate linear planar regimes from nonlinear planar regimes and nonlinear nonplanar regimes of motion. The predicted regimes compare rather favorably with recent experimental work on the nonlinear effects in nanotube and nanowire resonators. We also predict that whirling motions can easily occur within the parameter space of recent experimental work.

A sketch of a typical nano-oscillator of length L suspended above a trench is shown in Figure 1. The vertical deflection is w while the horizontal deflection is v, axial deformations are assumed to behave in a quasi-static manner.[20] Both deflections are measured relative to the undeformed position of the oscillator at a point x . The oscillator is assumed to be cylindrical with diameter d, suspended above a trench of height h, mass per unit length m, elastic modulus E, area moment I, and cross sectional area A. The combination of these properties results in bending rigidity EI and radius of gyration $(I/A)^{1/2}$. The nondimensional coupled partial differential equations which describe the deformations of a doubly clamped oscillator with a symmetric cross section are[21]

$$
\begin{aligned}
W_{,\tau\tau} + \frac{1}{\beta^4}W_{,XXXX} - \frac{1}{2R^2\beta^4}W_{,XX}\int_0^1 [W_{,X}{}^2 + V_{,X}{}^2]\,dX = F(X,\ \tau) \\
V_{,\tau\tau} + \frac{1}{\beta^4}V_{,XXXX} - \frac{1}{2R^2\beta^4}V_{,XX}\int_0^1 [W_{,X}{}^2 + V_{,X}{}^2]\,dX = 0
\end{aligned}
\qquad (1)
$$

where the nondimensional parameters relate the dimensional parameters in Figure 1 as follows

$$
\begin{aligned}
&W = w/h, \quad V = v/h, \quad D = d/h, \\
&X = x/L, \quad R^2 = \frac{I}{Ah^2}, \quad \tau = \omega_0 t
\end{aligned}
\qquad (2)
$$

and subscripts correspond to partial derivatives with respect to time, τ, or space, X (for example $(\cdot)_{,\tau} = \partial(\cdot)/\partial\tau$). The natural frequency of the oscillator is $\omega_0 = \beta^2((EI)/(l^4m))^{1/2}$ and β is a numerical factor depending on the eigenmode of the oscillator. For electrostatically excited devices,[1] the nondimensional force per unit length, $F(X, \tau)$, is a result of the capacitance between the oscillator and the gate electrode located at the base of the trench. To model this force, the oscillator is assumed to be an infinite conducting cylinder above the gate—an infinite conducting plane.[10,22,23] The force is nondimensionalized by the compliance of the oscillator, S, as well as the nondimensional parameters in eq 1. The applied gate voltage is $V_g(\tau) = V_{dc} + V_0\cos(\Omega\tau)$, where V_{dc} is the applied dc gate voltage, V_0 is the amplitude of the ac gate voltage, and Ω is the frequency of the ac gate voltage. Following the lead of ref 1, the force is nondimensionalized, and the dependence of $F(X, \tau)$ on the vibration, W, is neglected. This assumption can be shown to be valid so long as the vibration amplitudes are much smaller than the gap. However, as the gap size decreases, additional terms must be accounted for in the exciting force that can result in linear and nonlinear parametric excitation terms—this extension is the subject of ongoing work by the authors. For the present, we thus have

$$F(X,\ \tau) = \frac{-S\pi\varepsilon_0(V_g(\tau)/h)^2}{(1+W)[\ln(4(1+W)/D)]^2} \approx -\frac{S\pi\varepsilon_0(V_g(\tau)/h)^2}{[\ln(4/D)]^2} \approx -\frac{2S\pi\varepsilon_0(V_{dc}V_0/h^2)\cos(\Omega\tau)}{[\ln(4/D)]^2} \qquad (3)$$

where $S = L^4/\beta^4 EI$ is the modal compliance of the oscillator to a transverse, distributed load. Additionally, only the harmonic term is retained. The constant offset will apply initial tension. The effect of initial tension is discussed towards the end of this work. In the case of magnetomotive forcing,[5] the driving force $F(X, \tau) = i(\tau) \times B$, where B is the uniform applied magnetic field and an alternating voltage drives the time varying current, $i(\tau)$, through the oscillator. It can be shown that for sufficiently small oscillation amplitudes the magnetomotive forcing can also be modeled as an external, harmonic force, as in eq 3.

When the oscillator is driven near the resonance of the first bending mode, we assume that $W(X, \tau) = q_1(\tau)\varphi(X)$ and $V(X, \tau) = q_2(\tau)\varphi(X)$ where $\varphi(X)$ is the first eigenmode of a linear Bernoulli−Euler beam with clamped−clamped boundary conditions and is normalized such that $\int_0^1 \varphi^2(X)\ dX = 1$. It can be shown[24] that for the first eigenmode of a doubly clamped beam, $\beta = 4.73$. Substituting the assumed solution form into eq 1 and multiplying the resulting equation by $\varphi(X)$ and integrating over the length of the oscillator yields the following two-degree-of-freedom model

$$\begin{aligned} q_{1,\tau\tau} + \frac{1}{Q}q_{1,\tau} + q_1 + 8\alpha q_1[{q_1}^2 + {q_2}^2] &= -2F_0\cos(\Omega\tau) \\ q_{2,\tau\tau} + \frac{1}{Q}q_{2,\tau} + q_2 + 8\alpha q_2[{q_1}^2 + {q_2}^2] &= 0 \end{aligned} \qquad (4)$$

where $q_1(\tau)$ represents the dynamics of the oscillator in the plane of forcing and $q_2(\tau)$ represents the out-of-plane motion. Furthermore, the axial stretching induces a nonlinearity, α, which is given by

$$\alpha = \frac{1}{16R^2\beta^4}[\int_0^1 {\varphi_X}^2\ dX]^2 = \frac{151.3}{16R^2\beta^4} \qquad (5)$$

and the modal forcing amplitude F_0 is

$$F_0 = S\frac{\pi\varepsilon_0(V_{dc}V_0/h^2)}{(\ln(4/D))^2}\int_0^1 \varphi\ dX = 0.831S\frac{\pi\varepsilon_0(V_{dc}V_0/h^2)}{(\ln(4/D))^2} \qquad (6)$$

A modal damping term with quality factor Q is included in eq 4. Equation 5 shows that the stretching nonlinearity is responsible for coupling the in-plane and out-of-plane dynamics; without this nonlinearity the dynamics would be restricted to the forcing plane. The linear resonance frequency of the nano-oscillator is excited in eq 4 when $\Omega = 1$.

The mechanical motion of the resonator modulates its electronic conductance. In magnetomotively excited nanowires, this effect occurs due to electromagnetic induction.[2] In an electrostatically excited nanotube, the conductance change occurs due to the induced charge on the nanotube.[1] In either case, the measured current modulation is, to leading order, linearly proportional to the planar amplitude of motion.[16]

We consider a single-walled carbon nanotube (SWCNT) based oscillator and match our parameter values with those from ref 1. Particularly, we choose to consider a SWCNT of diameter 2.5 nm that is suspended over a 500 nm deep trench. These parameter values result in $D = 0.005$. We use a natural frequency of 5.02 MHz and a quality factor of $Q = 25$, these parameters are chosen to match device 2 discussed in Sazonova et al.[1] Since SWCNTs are thin-walled structures, the limiting case for the radius of gyration is assumed, $R^2 = D^2/4$. The nonlinear term from eq 5 is found to be $\alpha = 3023$ and the compliance is $S = 0.167$ m^2/N. (Due to uncertainty in the elastic modulus and area moment of a SWCNT oscillator, the measured natural frequency is used to determine the value of $\beta^4 EI/L^4 m$. The mass per unit length, m, of a 2.5 nm diameter SWCNT is approximately 6.0×10^{-15} kg/m which allows for the compliance, S, of the SWCNT to be calculated.) A dc gate voltage of $V_{dc} = 9$ mV is applied in all the simulation data presented. The quality factor and resonance frequency are found by fitting the linear response to match with Figure 3b of ref 1 ($V_0 = 8.8$ mV). Next, the hardening parameter α is found by matching the slope of the nonlinear amplitude response shown in Figure 3b of ref 1 (40 mV). The α value in turn uniquely determines the nanotube diameter, d (which falls in the range of measured nanotubes in ref 1), using eqs 2 and 5. The dc voltage, V_{dc}, is matched to the low frequency jump point in Figure 3b of ref 1.

For the particular parameter values shown above, the steady-state periodic solutions of eq 4 are computed in AUTO,[25] a powerful tool for continuation and bifurcation problems in dynamical systems. For low forcing voltages, the dynamics appear to be linear as the drive frequency is swept up and down across resonance. This is shown in Figure 2a when an alternating voltage $V_0 = 8.8$ mV is applied to the gate electrode. As the forcing voltage is increased to $V_0 = 20$ mV, a pair of saddle-node bifurcations occurs which results in the hysteretic jump behavior as the frequency is increased and then decreased. The resonance response bends to higher frequencies confirming that the stretching nonlinearity hardens the response, which matches the experimental results.[1,2] Experimental data for device 2 from ref 1 are shown as green diamonds.

As the alternating part of the gate voltage V_0 increases to 40 mV, another branch of nanotube motions is observed. As shown in red in Figure 2b, the planar branch becomes unstable and the in-plane amplitude is decreased when compared to the unstable planar solution. The out-of-plane amplitude is shown in Figure 2c. An examination of the phase of these motions reveals that this nonplanar solution represents three-dimensional elliptical whirling motion of the nanotube. While we do not show it in the figure, the nonplanar solution can also lose stability for a narrow range of frequencies via so-called torus bifurcations.[26] The experimental data from ref 1 is shown in Figure 2b for comparison. While the nonlinear response follows the nonlinear "backbone" well, the experimental results for $V_0 = 40$ mV shown in Sazonova et al.[1] do not appear to show whirling, at odds with the theoretical predictions. However, given the limited number of parameter values that can be accurately inferred from the details in ref 1, the deviation between the theoretical

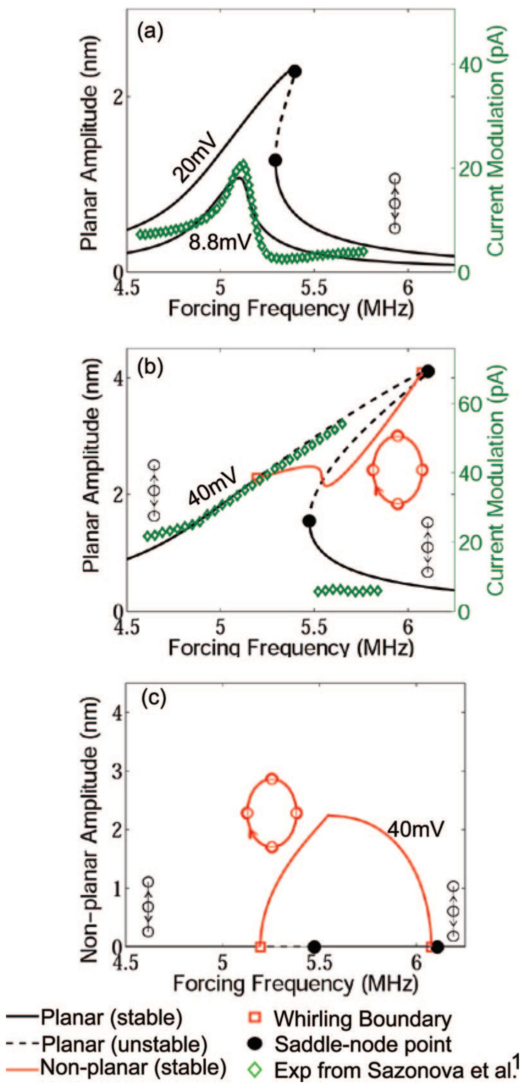

Figure 2. A comparison of model prediction and the experimental results from Sazonova et al.[1] Periodic solutions of eq 4 are found using AUTO[25] using device parameters deduced from device 2 results from Sazonova et al.,[1] particularly $Q = 25$ and $\alpha = 3023$. Black solid lines are stable planar solutions while dashed black lines are unstable planar solutions, red solids lines correspond to stable whirling, nonplanar motions of the nanotube. The linear stability of all solutions is determined in AUTO via Floquet multipliers. The displacement is measured at the middle of the nanotube span. (a) The in-plane amplitude of motion for varying forcing voltages. Initially only a planar motion is present ($V_0 =$ 8.8 mV); at higher voltages ($V_0 = 20$ mV) a nonlinear hysteresis or a jump occurs as the drive frequency is varied. (b) The in-plane amplitude for $V_0 = 40$ mV. A region of whirling occurs, shown in red. While the tube is whirling, the in-plane amplitude is decreased when compared to the unstable planar solution. (c) The out-of-plane amplitude of motion for $V_0 = 40$ mV . Outside a certain frequency bandwidth, no out-of-plane motion exists; however, within the bandwidth, the whirling amplitude quickly grows to reach a maximum value.

results and experimental data is reasonable. Even so, as we will shortly see, with increased driving voltages and higher Q-factors it is very hard to avoid whirling dynamics in such resonators.

We now use the method of first-order averaging[26] to find *analytical expressions* for the parameter values that lead to hysteretic jumps in the planar motion as well as the onset of whirling. In this mathematical asymptotic technique the slow time scale system dynamics are approximated by averaging over fast time the forcing, damping, closeness to linear resonance, and nonlinearity which are all considered perturbations to an undamped harmonic oscillator. We assume the response to be of the form $q_1(\tau) = A_1(\tau)\cos(\Omega\tau + \beta_1(\tau))$ and $q_2(\tau) = A_2(\tau)\cos(\Omega\tau + \beta_2(\tau))$, where $A_1(\tau)$, $A_2(\tau)$, $\beta_1(\tau)$, and $\beta_2(\tau)$ are all slowly varying functions of time[26] where the time evolution of amplitude and phase are governed by the following equations derived from first-order averaging

$$\begin{aligned}
A_{1,\tau} &= \frac{1}{\Omega}\Big[-\frac{1}{2Q}A_1(\tau) + \alpha A_1(\tau)A_2{}^2(\tau)\sin[2(\beta_1(\tau)-\beta_2(\tau))] + \\
&\qquad F_0\sin\beta_1(\tau)\Big] \\
A_1\beta_{1,\tau} &= \frac{1}{\Omega}\Big[-A_1(\tau)\frac{\sigma}{2} + 3\alpha A_1{}^3(\tau) + \alpha A_1 A_2{}^2(\tau)\{2 + \\
&\qquad \cos[2(\beta_2(\tau)-\beta_1(\tau))]\} + F_0\cos\beta_1(\tau)\Big] \\
A_{2,\tau} &= \frac{1}{\Omega}\Big[-\frac{1}{2Q}A_2(\tau) + \alpha A_2(\tau)A_1{}^2(\tau)\sin[2(\beta_2(\tau)-\beta_1(\tau))]\Big] \\
A_2\beta_{2,\tau} &= \frac{1}{\Omega}\Big[-A_2(\tau)\frac{\sigma}{2} + 3\alpha A_2{}^3(\tau) + \alpha A_1{}^2(\tau)A_2(\tau)\{2 + \\
&\qquad \cos[2(\beta_1(\tau)-\beta_2(\tau))]\}\Big]
\end{aligned} \tag{7}$$

where $\sigma \equiv \Omega^2 - 1$ measures the detuning between the forcing frequency (Ω) and the linear resonance frequency (which is scaled to 1 in the nondimensionalization). Equilibrium points of these differential equations correspond to steady harmonic motions.

To predict analytically the detuning (or equivalently the drive frequency) σ_{SN} and excitation magnitude F_{0SN} at which an amplitude jump (or saddle-node bifurcation) occurs in planar motion, we first set the left-hand sides of eq 7 to zero for steady-state motion and specify $A_2 = 0$ for planar motion. A jump or saddle-node bifurcation occurs when the slope with respect to σ of the amplitude A_1 response becomes unbounded, $dA_1/d\sigma = \infty$. This requirement leads to the following analytical algebraic equations whose solutions determine σ_{SN}, F_{0SN}, and A_{1SN}

$$\begin{aligned}
&\frac{\sigma_{SN}}{\alpha} = 6A_{1SN}^2 + 2\sqrt{\left(\frac{F_{0SN}}{\alpha}\right)^2\frac{1}{6A_{1SN}^2} - \frac{1}{4(Q\alpha)^2}} \\
&-36\frac{1}{4(Q\alpha)^2}(A_{1SN}^2)^4 + 36\left(\frac{F_{0SN}}{\alpha}\right)^2(A_{1SN}^2)^3 - \left(\frac{F_{0SN}}{\alpha}\right)^4 = 0
\end{aligned} \tag{8}$$

where A_{1SN} is the planar amplitude at which the jump occurs. Given a frequency detuning σ_{SN}, it becomes possible using eq 8 to determine the F_{0SN} and A_{1SN}.

We now determine the conditions required for the onset of nonplanar whirling motions ($A_1 \neq 0$ and $A_2 \neq 0$). The nonplanar branch arises through a pitchfork bifurcation from the planar solution branch.[17] At the pitchfork point, the determinant of the Jacobian matrix of the linearized system about the equilibrium must vanish.[26] Applying this requirement to an equilibrium point of eq 7 we find that the locus of drive frequencies (σ_{PF}) and driving force amplitudes

F_{OPF} at which a pitchfork bifurcation occurs off the planar solutions is given by the following algebraic equations

$$A_{1PF}^2 = \frac{\frac{\sigma_{PF}}{\alpha} \pm \sqrt{\frac{1}{4}\left(\frac{\sigma_{PF}}{\alpha}\right)^2 - \frac{3}{4}\frac{1}{(Q\alpha)^2}}}{3}$$

$$\left[\frac{1}{4}\left(\frac{\sigma_{PF}}{\alpha}\right)^2 + \frac{1}{4(Q\alpha)^2}\right]A_1 - 3\frac{\sigma}{\alpha}A_1 + 9A_1 = \left(\frac{F_0}{\alpha}\right)^2 \qquad (9)$$

where A_{1PF} is the planar amplitude at which the pitchfork occurs. Both the conditions for the onset of jump phenomena eq 8 and for the onset of nonplanar whirling eq 9 are expressed in terms of experimentally verifiable quantities. The quality factor Q can be determined from linear frequency response measurements while the forcing F_0 and detuning σ are varied experimentally. The nonlinear stretching term can also be determined by fitting the nonlinear resonance response to the model.

Equations 8 and 9 suggest that the saddle-node (jumps in planar amplitude response) bifurcations and pitchfork bifurcations (onset of nonplanar whirling) can be represented as loci in a two-dimensional parameter space of $(\sigma/\alpha)^{1/2}$ and F_0/α. The loci depend on on the particular value of $Q\alpha$. This characterization allows for the creation of a "universal" parameter space diagram on which different device designs can be conveniently compared in terms of their nonlinear and nonplanar behavior. For instance in Figure 3a the loci of the saddle-node bifurcations are plotted in terms of scaled deviation of forcing and natural frequency $(\sigma/\alpha)^{1/2}$ and driving force F_0/α. These loci are plotted for different $Q\alpha$ values: $Q\alpha = \infty$ for a hypothetical oscillator with $Q = \infty$, $Q\alpha = 62500$ based on the experimental results of ref 2 and $Q\alpha = 75600$ based on the experimental results of ref 1. In Figure 3a the experimentally measured loci from ref 1 and ref 2 are also plotted. It is clear that the measured and predicted loci match fairly well. Moreover as the Q factor of resonator increases, the jump phenomena occur at lower driving forces and over larger frequency bandwidths.

In Figure 3b the loci of the pitchfork bifurcations that signify the onset of nonplanar whirling motions are plotted for $Q\alpha = 75600$, $Q\alpha = 62500$, and $Q\alpha = \infty$. Figure 3b shows that for device parameters taken from ref 1 that the onset of nonplanar whirling is expected near the forcing voltages reported in ref 2. Moreover as the Q factor of the resonance increases, nonplanar dynamics occur for lower driving forces and over a wider range of excitation frequencies. The whirling predictions may require a caveat—the experimental device in ref 5 as an example is not a nanotube but rather possesses a rectangular cross section for which the resonance frequencies of the in-plane and out-of-plane modes are not closely spaced. This issue of nonsimilar in-plane and out-of-plane resonance frequencies is addressed next.

The model discussed above is for an idealized oscillator (a) without initial slack or initial tension and (b) assumes that the in-plane and out-of-plane resonance frequencies are identical. It is interesting to ask how the predictions are affected when these realistic effects are included in the model. The influence of initial tension can be easily included

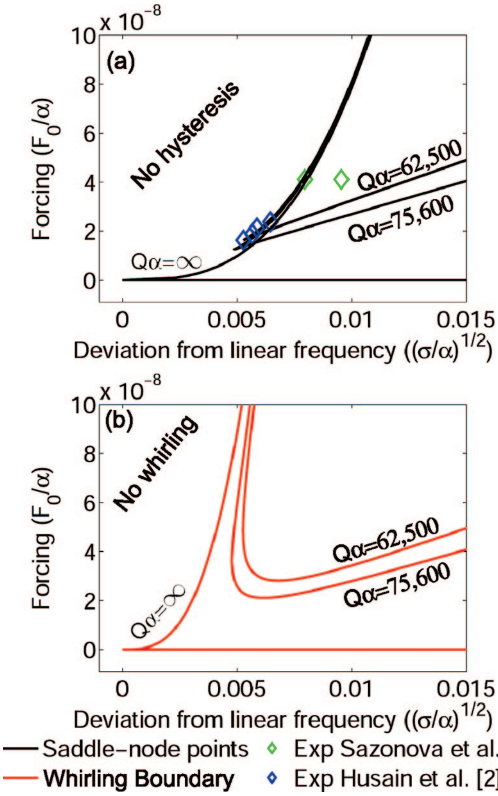

Figure 3. Parameter space diagram showing loci of parameters where (a) jumps occur due to saddle-node bifurcations and (b) where whirling begins and ends due to pitchfork bifurcations in the averaged equations. The abscissa is the scaled deviation away from linear resonance and the ordinate axis is the scaled forcing. The locus corresponding to $Q\alpha = 75600$ corresponds to the theoretical prediction based on parameters from ref 1 while the locus for $Q\alpha = 62500$ matches the parameters of ref 2. Additionally, the case of no damping ($Q\alpha = \infty$) is also included, where both hysteresis and whirling occur for *all* forcing voltages. The green diamonds are experimental data from ref 1 while the black diamonds are experimental data from ref 2.

into the model using a tensioning term in eq 1.[20] The net effect of increased tension will be to increase the resonance frequency ω_0 and decrease the compliance S. Thus initial tension can be easily incorporated into the model and has no effect following eq 4; thus the dimensionless parameter regimes discussed remain unchanged.

The presence of initial slack on the other hand implies that the resonator is not initially straight. Also, recall that we have neglected the constant component of gate forcing in this work. This component would also introduce an initial sag in the nanotube. Additionally, compressive forces from fabrication may initially buckle the beam, resulting in initial curvature. If the initial sag or curvature becomes significantly large, eq 1 needs to be modified to that of an initially curved beam[27,28] which then introduces quadratic nonlinearities in addition to the cubic stretching nonlinearities. In principle, these terms are unlikely to influence the onset of whirling but are expected to modify the dynamics of whirling once it it is initiated. The more important effect of initial slack, or, for that matter, other fabrication imperfections, is that the eigenmodes of the oscillator become fixed in space and an eigenmode can no longer be assumed to lie along the plane of forcing to start with. Another important effect of initial slack and other imperfections is that the two eigenmodes need not have the same resonance frequency. This *internal mistuning* is expected to influence the boundaries in parameter space where the different bifurcations occur;[19] qualitatively the results will be similar to those predicted here so long as this internal mistuning is small. As a rough estimate, so long as the resonance bandwidths of the two orthogonal eigenmodes overlap, it should be possible to find regions in the forcing amplitude-drive frequency space where whirling motions set in. In summary, the theoretical predictions made in this article will continue to hold qualitatively even in the presence of realistic perturbative effects, so long as the initial curvatures and internal mistuning remain sufficiently small.

In conclusion, we have shown that the mechanical stretching nonlinearity greatly influence electromechanical response of nanowire- and nanotube-based oscillators, and they also open up several opportunities for exploiting these electromechanical nonlinearities. The existence of multiple planar oscillation state and jump phenomena have been observed and predicted by others;[1,2,15] however, the present work provides convenient analytical equations to predict the dependence on scaled system parameters. The predicted onset of nonplanar whirling opens up interesting modalities for such nano-oscillators. For instance, it can be used as an embedded overload protection mechanism; when the driving force exceeds a critical value, whirling sets in and current modulation suddenly decreases. Alternatively, the nonplanar whirling can be used as an amplitude limiting mechanism in a self-resonating electromechanical oscillator.

In this work we have focused on the *onset* of nonplanar whirling motions in nanotube and nanowire oscillators. However many other nonplanar motions are known to occur in macroscopic guitar-like strings that are forced in a single plane. These include amplitude modulated whirling motions and torus doublings[17] as well as Si'lnikov chaos.[29] Clearly the onset and use of nonplanar motions in nanotube and nanowire resonators can open up interesting applications of such devices in amplitude and frequency modulated signal processing as well as chaotic encryption.

Acknowledgment. The first author would like to acknowledge support from the Department of Energy Computational Science Fellowship Program of the Office of Science and National Nuclear Security Administration in the Department of Energy under contract DE-FG02-97ER25308. Additionally the authors acknowledge support from the National Science Foundation NIRT Grant No. CCF-05-6660.

References

(1) Sazonova, V.; Yaish, Y.; Ustunel, H.; Roundy, D.; Arias, T. A.; McEuen, P. A tunable carbon nanotube electromechanical oscillator. *Nature* **2004**, *431*, 284–287.
(2) Husain, A.; Hone, J.; Postma, H. W. Ch.; Huang, X. M. H.; Drake, T.; Barbic, M.; Scherer, A.; Roukes, M. L. *Appl. Phys. Lett.* **2003**, *83*, 1240–1242.
(3) Garcia-Sanchez, D.; San Paulo, A.; Esplandiu, M. J.; Perez-Murano, F; Forró, L.; Aguasca, A.; Bachtold, A. *Phys. Rev. Lett.* **2007**, *99*, 085501.
(4) Peng, H. B.; Chang, C. W.; Aloni, S.; Yuzvinsky, T. D.; Zettl, A. *Phys. Rev. Lett.* **2006**, *97*, 087203.
(5) Kozinsky, I.; Bargatin, H. W. Ch.; Roukes, M. L. *Appl. Phys. Lett.* **2006**, *88*, 253101.
(6) Witkamp, B.; Poot, M.; van der Zant, H. S. J. *Nano Lett.* **2006**, *6*, 2904–2908.
(7) Jensen, K.; Weldon, J.; Garcia, H.; Zettl, A. *Nano Lett.* **2007**, *7*, 3508–3511.
(8) Rueckes, T.; Kim, K.; Joselevich, E.; Tseng, G. Y.; Cheung, C.-L.; Lieber, C. M. *Science* **2000**, *289*, 94–97.
(9) Sharos, L. B.; Raman, A.; Crittenden, S.; Reifenberger, R. *Appl. Phys. Lett.* **2004**, *84*, 4638–4640.
(10) Poot, M.; Witkamp, B.; Otte, M. A.; van der Zant, H. S. J. *Phys. Status Solidi B* **2007**, *244*, 4252–4256.
(11) Zalamea, L.; Pipes, R. B. *J. Nanosci. Nanotechnol.* **2006**, *6*, 1177–1181.
(12) Ustunel, H.; Roundy, D.; Arias, T. A. *Nano Lett.* **2005**, *5* (3)), 523–526.
(13) Kozinksy I. *Nonlinear Nanomechanical Systems*. PhD thesis, California Institute of Technology, 2007.
(14) Postma, H. W. Ch.; Kozinsky, I.; Husain, A.; Roukes, M. L. *Appl. Phys. Lett.* **2005**, *86*, 223105.
(15) Kozinsky, I.; Bargatin, H. W. Ch.; Kogan, O.; Husain, A.; Roukes, M. L. *Phys. Rev. Lett.* **2007**, *99*, 207201.
(16) Sazonova. V. *A tunable carbon nanotube resonator*. PhD thesis, Cornell University, 2006.
(17) Bajaj, A. K.; Johnson, J. M. *Philos. Trans. R. Soc. London* **1992**, *338*, 1–41.
(18) Molteno, T. C.; Tufillaro, N. B. *Am. J. Phys.* **2004**, *79*, 1157–1169.
(19) Ho, C.-H.; Scott, R. A.; Eisley, J. G. *Int. J. Non-Linear Mech.* **1975**, *10*, 113–127.
(20) Nayfeh, A. H.; Mook, D. T. *Nonlinear Oscillations*; John Wiley & Sons: New York, 1995.
(21) Ho, C.-H.; Scott, R. A.; Eisley, J. G. *J. Sound Vib.* **1976**, *47*, 333–339.
(22) Scott. W. T. *The Physics of Electricity and Magnetism*; John Wiley and Sons: New York, 1959.
(23) Suydam. V. A. *Fundamentals of Electricity and Magnetism*; D Van Nostrand Company: New York, 1940.
(24) Meirovitch, L. *Principles and Techniques of Vibrations*; Prentice Hall: Upper Saddle River, NJ, 1997.
(25) Doedel, E. J. *AUTO 07P: Continuation and Bifurcation Software for Ordinary Differential Equations*, http://indy.cs.concordia.ca/auto, 2006.
(26) Wiggins, S. *Introduction to Applied Nonlinear Dynamical Systems and Chaos*; Springer-Verlag: New York, 1990.
(27) Nayfeh, A. H.; Balachandran, B. *Appl. Mech. Rev.* **1989**, *42*, S175−S201.
(28) Lacarbonara, W; Arafat, H N; Nayfeh, A H *Int. J. Non-linear Mech.* **2005**, *40*, 987–1003.
(29) O′Reilly, O M *Int. J. Non-linear Mech.* **1993**, *28*, 337–351.

NL073406J